# New Method to Calculate Mode Conversion Coefficients in SI Multimode Optical Fibers

J. Zubia, G. Durana, G. Aldabaldetreku, J. Arrue, M. A. Losada, and M. Lopez-Higuera

***Abstract*—A simple method is proposed for the experimental calculation of the mode conversion coefficients in multimode optical fibers. It only requires observing the far-field output pattern from a fixed length of fiber as the launching angle changes, as well as the intersection point between two far-field output patterns corresponding to two different input angles. The results obtained with this method are quite insensitive to small variations of the experimental parameters. A good agreement between theoretical and experimental results is also found.**

***Index Terms*—Mode conversion coefficients, mode coupling, multimode optical fiber, plastic optical fiber (POF).**

## I. Introduction

ALTHOUGH single-mode fibers offer better transmission properties since their bandwidth is superior, multimode fibers have several advantages; for example, they impose less stringent constraints on the light source (even luminescent diodes are suitable for transmission through a multimode fiber), and their large dimensions compared with those of single-mode fibers relax the tolerances required for connection and splicing. As a consequence, most of the devices, components and tools (lasers, detectors, connectors, etc.) used in multimode-based systems are substantially cheaper than those used in single-mode systems, which reduces the overall cost of the system, especially in access networks and local area networks (LANs).

System cost is not only sometimes the primary factor when designing a fiber-based system, but it also establishes the bit rate through the optical fiber. As a matter of fact, the demand for low-cost high-bandwidth communications in short and medium distances from different sectors of society is continuously increasing. Optical fibers made of polymer [plastic optical fibers (POFs)] have become increasingly popular due to their growing utility [1], [2]. Recently, they have found an application as a high-bandwidth communication medium for short distances, thanks to successive improvements in their physical properties [3]–[5].

Optical fiber bandwidth, which limits the data transmission speed [6], is greatly influenced by differential mode attenuation [7] as well as by mode-coupling effects [8]. The strong mode coupling observed in step-index optical fibers (SI-OF) reduces modal dispersion, and leads to a square-root dependence of the bandwidth on the fiber length instead of the expected linear dependence if mode coupling did not occur [9]. Because of the influence that mode coupling has on fiber bandwidth and on other related properties of optical fibers, it becomes necessary to have methods to obtain the rate of mode coupling in optical fibers [10].

To give a qualitative account of the mode coupling rate, that is, of the power transfer occurring between modes, the coupling coefficient is considered [11]–[14]. This coefficient measures, in real optical fibers, the mode-coupling rate owing to fiber impurities and inhomogeneities introduced during their manufacturing process, or to external factors such as external bends.

The method proposed by Gambling *et al.* has been considered by many authors [15] to calculate the mode conversion coefficient $D$ from Gloge's coupled-power flow equation [16], [17]. The method is quite simple, but it involves observing the far-field output pattern for various fiber lengths at different launching angles, which must be accurately measured [10].

The present paper offers an alternative method to that proposed by Gambling *et al.* We show that the mode conversion coefficient $D$ can be obtained from the observation of the far-field output pattern over a fixed length of optical fiber as the angle of incidence of a narrow laser beam changes. The results of the proposed method have been tested with MegaEska POFs,[1] although the method is suitable for any kind of SI multimode optical fiber.

The structure of the paper is as follows. First, a theoretical background is presented, which is necessary to understand the basis of the method, which is explained afterwards. Then, the experimental setup is explicated, to follow with the application of the method to multimode plastic optical fibers. The results obtained for these optical fibers are discussed. Finally, we finish by giving the main conclusions derived from the method.

## II. Theory

Our starting point is Gloge's coupled-power flow equation, assuming that, in a multimode optical fiber, mode coupling occurs primarily between the nearest neighboring modes. We have

$$\frac{\partial P(\theta, z)}{\partial z} = -A\theta^2 P(\theta, z) + \frac{D}{\theta}\frac{\partial}{\partial \theta}\left(\theta \frac{\partial P}{\partial \theta}\right) \qquad (1)$$

Manuscript received July 16, 2002; revised October 28, 2002. This work was supported by the Universidad del País Vasco-Euskal Herriko Unibertsitatea and by the Ministerio de Ciencia y Tecnología under projects 1/UPV/EHU00147.345-TA-8035/200 and TIC2000-059.

J. Zubia, G. Durana, G. Aldabaldetreku, and J. Arrue are with the Departamento de Electronica y Telecomunicaciones, ETSI de Bilbao, Universidad del Pais Vasco, Bilbao, Spain (e-mail: jtpzuzaj@bi.ehu.es).

M. A. Losada is with the Centro Politecnico Superior, Universidad de Zaragoza, Zaragoza, Spain.

M. Lopez-Higuera is with the Universidad de Cantabria, Santander, Spain.

Digital Object Identifier 10.1109/JLT.2003.809556

[1]From Mitsubishi Rayon Co. Ltd. [Online] Available: http://www.mrc.co.jp/english/.

where

| | |
|---|---|
| $P(\theta, z)$ | power distribution in the fiber; |
| $D$ | mode conversion coefficient; |
| $A$ | second order multiplicative factor in the series expansion of the power loss coefficient; |
| $\alpha$ | $\alpha(\theta) = \alpha_0 + A\theta^2 + \cdots$. |

A solution for the differential equation can be found by using the variable separation technique. The result is the following:

$$P(x, z) = \sum_{n=0}^{\infty} K_n L_n(x) \exp(-1/2x) \exp(-\gamma_n z) \quad (2)$$

where $x = (A/D)^2\theta^{1/2}$, $L_n(x)$ are Laguerre polynomials, $\gamma_n$ is defined as $\gamma_n = 2(2n+1)(AD)^{1/2}$, and the expansion coefficient $K_n$ is determined from the input conditions. Now we consider the special case of a plane wave launched at an angle $\theta_0$ with the fiber axis ($x_0 = (A/D)^{1/2}\theta_0^2$). For this power distribution, $P(x, 0)$ is the Dirac delta function $\delta(x - x_0)$. This launching condition, combined with the orthogonal relations for the Laguerre polynomials, enables us to obtain a convenient expression for the output power distribution [10]

$$P(x, z) = \exp\left(-\frac{x_0 + x}{2}\frac{1+\exp(-bz)}{1-\exp(-bz)}\right) \times \left(\frac{\exp(-1/2bz)}{1-\exp(-bz)}\right) I_0\left[\frac{(4x_0x)^{1/2}\exp(-1/2bz)}{1-\exp(-bz)}\right] \quad (3)$$

where $b = 4(AD)^{1/2}$ and $I_0$ is the modified Bessel function of order zero.

In order to illustrate the basis of the method, we consider a fixed fiber length $L$. At the fiber input, we launch a plane wave making an angle $\theta_{01}$ with the fiber axis. The output power distribution is depicted in Fig. 1. Now we consider the same input plane wave, but at a different launching angle $\theta_{02}$. The new output power distribution is also depicted in Fig. 1. As can be seen from the figure, both curves intersect at the output angle $\theta_{0c}$. This condition is set in the following equality:

$$P(x_{01}, L) = P(x_{02}, L) \quad (4)$$

or, equivalently

$$\begin{aligned} P(x_{01}, L) &= \exp\left(-\frac{x_{01}}{2}\frac{1+\exp(-bL)}{1-\exp(-bL)}\right) \times I_0\left[\frac{(4x_{01}x_{0c})^{1/2}\exp(-1/2bL)}{1-\exp(-bL)}\right] \\ &= \exp\left(-\frac{x_{02}}{2}\frac{1+\exp(-bL)}{1-\exp(-bL)}\right) \times I_0\left[\frac{(4x_{02}x_{0c})^{1/2}\exp(-1/2bL)}{1-\exp(-bL)}\right] \\ &= P(x_{02}, L). \end{aligned} \quad (5)$$

If we define the new variables $v = (AD)^{1/2}$ and $u = (A/D)^{1/4}$, (5) can be rewritten as

$$\exp\left(-\frac{u^2\theta_{01}^2}{2}\coth(2vL)\right) I_0\left[\frac{u^2\theta_{01}\theta_{0c}}{\sinh(2vL)}\right] = \exp\left(-\frac{u^2\theta_{02}^2}{2}\coth(2vL)\right) I_0\left[\frac{u^2\theta_{02}\theta_{0c}}{\sinh(2vL)}\right]. \quad (6)$$

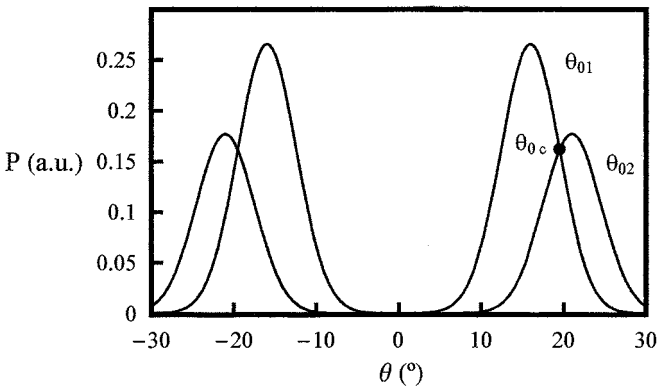


Fig. 1. Output angular power distributions for a fixed length of fiber $L = 3$ m and two launching angles $\theta_{01} = 16.5°$ and $\theta_{02} = 21.5°$, derived from Gloge's coupled-power flow equation.

Considering that $\theta_{01}$, $\theta_{02}$, $\theta_{0c}$, and $L$ are experimentally measurable quantities, there are only two unknowns: $u$ and $v$. Thus, we need another equation to be able to find the values of the variables $u$ and $v$. For this purpose, we notice that the transition occurring at the output angular power distribution from a ring-shaped pattern into a disk-shaped pattern takes place at an angle $\theta_{0m}$ obtained from the following condition [10]:

$$\frac{\partial^2 P(\theta, z)}{\partial\theta^2} = 0 \quad \text{at} \quad \theta = 0. \quad (7)$$

This criterion applied to the power distribution given by (3) leads to

$$(A/D)^{1/4}\theta_{0m} = \left\{\frac{1-\exp[-8(AD)^{1/2}L]}{2\exp[-4(AD)^{1/2}L]}\right\}^{1/2} \quad (8)$$

or

$$u = \frac{1}{\theta_{0m}}\sqrt{\sinh(4vL)}. \quad (9)$$

If we now substitute this expression for $u$ in (6), we obtain

$$\begin{aligned} &\exp\left(-\left(\frac{\theta_{01}}{\theta_{0m}}\right)^2\cosh^2(2vL)\right) \times I_0\left[2\left(\frac{\theta_{01}\theta_{0c}}{\theta_{0m}^2}\right)\cosh(2vL)\right] \\ &= \exp\left(-\left(\frac{\theta_{02}}{\theta_{0m}}\right)^2\cosh^2(2vL)\right) \times I_0\left[2\left(\frac{\theta_{02}\theta_{0c}}{\theta_{0m}^2}\right)\cosh(2vL)\right]. \end{aligned} \quad (10)$$

We finally define the dimensionless quantities $l_1 = (\theta_{01}/\theta_{0m})^2$, $l_2 = (\theta_{02}/\theta_{0m})^2$, $m_1 = (\theta_{01}\theta_{0c})/\theta_{0m}^2$ and $m_2 = (\theta_{02}\theta_{0c})/\theta_{0m}^2$, and the variable $w = \cosh(2vL)$. Then, (10) yields

$$\exp\left(-l_1w^2\right) I_0[2m_1w] = \exp\left(-l_2w^2\right) I_0[2m_2w] \quad (11)$$

where $l_1$, $l_2$, $m_1$, and $m_2$ are experimentally obtainable quantities. Thus, if we calculate $w$ numerically from the above equation, we can obtain $u$ and $v$ by using the following relations:

$$\begin{aligned} v &= \frac{1}{2L}\operatorname{arccosh} w \\ u &= \frac{1}{\theta_{0m}}\sqrt{2\left(w^2-1\right)^{1/2}w}. \end{aligned} \quad (12)$$

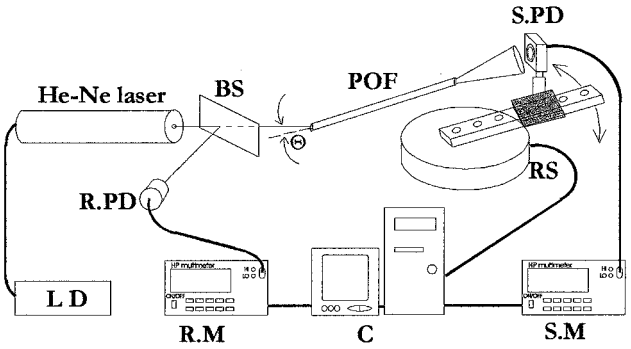


Fig. 2. Experimental setup for the determination of the transition angle $\theta_{0m}$ and the angle $\theta_{0c}$ corresponding to the intersection point between two output angular power distributions. BS—beam splitter. R.PD—reference photodetector. S.PD—signal photodetector. RS—rotating stage. LD—laser driver. R.M—reference multimeter. S.M—signal multimeter. C—computer.

It should be noted that this method does not make use of any approximation, and not even to determine $u$ and $v$: they can be calculated from their definition. However, if we assume that $2vL \ll 1$, we can expand $\cosh(2vL)$ in a Taylor series, and write $v$ as follows:

$$v = \frac{1}{L}\sqrt{\frac{w-1}{2}}. \tag{13}$$

This Taylor series expansion proves justified once we obtain the results.

From $u$ and $v$, the coefficients $A$ and $D$ are calculated by means of the following expressions:

$$A = u^2 v, \qquad D = \frac{v}{u^2}. \tag{14}$$

The exposed method completely determines $A$ and $D$ if we measure the transition angle $\theta_{0m}$ between two output angular power distributions corresponding to the launching angles $\theta_{01}$ and $\theta_{02}$.

## III. Experiment

Fig. 2 shows the experimental setup employed to calculate the parameters required by the method.

A 543-nm-wavelength He–Ne laser is used to launch the plane waves. The laser beam crosses a beam splitter in order to obtain a reference signal and cancel the laser light intensity fluctuations. One of the two light beams impinges on the fiber input face at an angle $\theta_0$. The light that exits the POF is collected by an automatic rotating silicon photodetector whose active area is $0.12\ \text{mm}^2$, moving in the range of angles $-30° \leq \theta \leq 30°$, and placed approximately 3.1 cm away from the POF output.

The fiber input end stands on a rotatory stage in order to control the incidence angle. Two multimeters, attached to the reference and signal detectors, send their measurements to a computer, which stores all the data in a file for further processing. The process described here is fully automated.

## IV. Results and Discussion

We have applied this method to a sample of Eska Premier plastic optical fiber of length $L = 3$ m (Mitsubishi Rayon; $d_{\text{core}} = 0.98$ mm, $n_{\text{core}} = 1.492$, $NA = 0.5$), although the method can be applied to any fiber length. We prefer to use fiber lengths that can be maintained straight in the experimental setup to avoid the introduction of additional mode coupling as a consequence of winding the fibers around reels. Using the experimental setup described above, several measurements were carried out at different input angles to determine both the transition angle $\theta_{0m}$ and the angle $\theta_{0c}$ corresponding to the intersection point between two output angular power distributions.

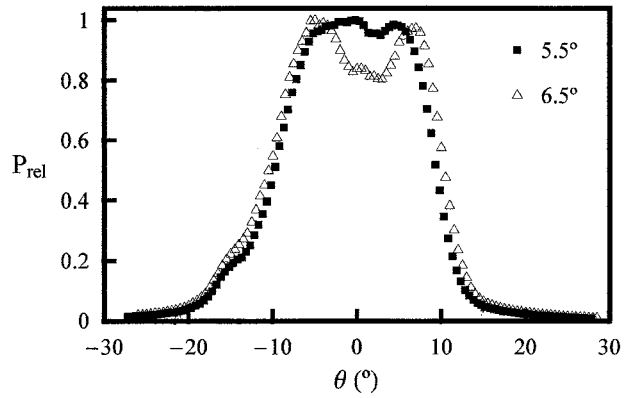


Fig. 3. Experimental output angular power distributions for the launching angles $\theta_0 = 5.5°$ and $\theta_0 = 6.5°$. The transition from a ring-shaped pattern to a disk-shaped pattern occurs at $\theta_0 = 5.5°$.

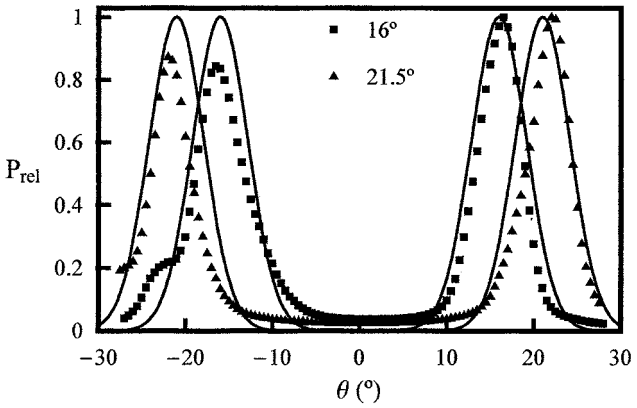


Fig. 4. Comparison between the output power distributions obtained from Gloge's model (continuous lines) and the experimental ones (square and triangular data points). The output power distributions correspond to the input angles $\theta_{01} = 16°$ and $\theta_{02} = 21.5°$.

For the considered POF and fiber length, the transition in the output angular power distribution from a ring-shaped pattern to a disk-shaped pattern happens approximately at an input angle of $\theta_{0m} = 5.5°$ (Fig. 3). For input angles just above the transition angle, the output power distribution is a double-peaked curve, as can be seen in Fig. 3 for an input angle of $\theta_0 = 6.5°$.

Fig. 4 represents the output power distributions for the input angles $\theta_{01} = 16°$ (square data points) and $\theta_{02} = 21.5°$ (triangular data points), although the choice of the input angles is arbitrary. The intersection point between both curves, which have been read out directly from the data, occurs approximately at an output angle of $19.5°$ ($\theta_{0c} = 19.5°$).

From this experimental data, we calculate $l_1$, $l_2$, $m_1$ and $m_2$ ($l_1 = 8.46$, $l_2 = 15.28$, $m_1 = 10.31$, $m_2 = 13.869$) and, after

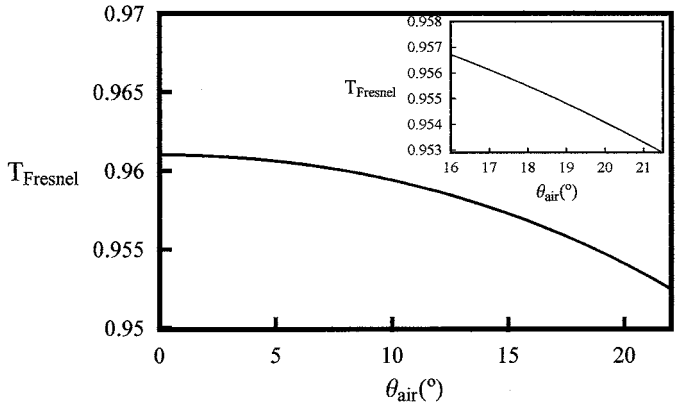


Fig. 5. Graphical representation of the Fresnel scalar transmission coefficient at the air-core interface as a function of the incidence angle. Small changes in the coefficient are observed in the range from $\theta_{01} = 16°$ ($T_{\text{Fresnel}} = 0.9567$) to $\theta_{02} = 21.5°$ ($T_{\text{Fresnel}} = 0.9529$).

having solved (11) numerically, we find the following solution for the coefficients $A$ and $D$ (wavelength of light =543 nm):

$$A = 1.37 \text{ rad/m}, \qquad D = 7.5\ 10^{-4} \text{ rad}^2/\text{m}. \tag{15}$$

In the calculations, we have neglected the dependence of the Fresnel transmission coefficient on the incidence angle at the input face of the fiber. Thus, we have not considered a possible correction factor for the input power distribution within the fiber core which, for each incidence angle, accounts for the Fresnel reflection occurring on the fiber input face. This small neglect is justified from Fig. 5, which shows the dependence of the Fresnel transmission coefficient ($T_{\text{Fresnel}}$) on the incidence angle when no polarization dependence exists (scalar approximation). For the input angle of 16°, the Fresnel coefficient is 0.9567, whereas for the input angle of 21.5°, it is 0.9529. Thus, both coefficients are approximately the same, and therefore the power that penetrates into the fiber core is the same as well; this fact holds true provided that the area covered by the laser beam is smaller than that of the fiber core for both input angles.

If the laser beam completely covers the fiber core, then the power coupled into the fiber depends on the launching angle. To take it into account, we have to consider a correction factor. For this purpose, let $P_{01}$ be the power that penetrates into the fiber core when the input angle is $\theta_{01}$ and $P_{02}$ be the input power within the fiber core when the input angle is $\theta_{02}$. We now define the dimensionless quantity $K = P_{01}/P_{02}$. Then (4) turns out to be

$$K \exp(-l_1 w^2) I_0[2m_1 w] = \exp(-l_2 w^2) I_0[2m_2 w]. \tag{16}$$

Note that if the power coupled into the fiber core does not change for two different launching angles, then $P_{01} = P_{02}$ and $K = 1$, so we recover (11). $K$ is equal to $\cos\theta_{01}/\cos\theta_{02}$ provided that the incident beam is an infinite uniform plane wave. However, the $\text{TEM}_{00}$ mode of our laser beam has a Gaussian power distribution, so the relation between $P_{01}$ and $P_{02}$ is not so simple. Thus, in order to numerically solve (16), we need to determine $K$ experimentally. This can be done by taking two fixed launching angles ($\theta_{01} = 16°$ and $\theta_{02} = 21.5°$ in our case) into a short length of optical fiber, and by measuring the output power in both cases. In our measurements, $K$ turned out to be 1.15 ($K = P_{16.5°}/P_{21.5°}$). These two measurements were also made over the fiber under test ($L = 3$ m), and the same result was obtained for $K$.

However, small deviations between the input angle $\theta_0$ and the real one may happen, mainly because the input fiber surface does not remain perpendicular to the fiber axis. And in the same manner, the values of the parameters $\theta_{0c}$, $\theta_{0m}$, and $K$ considered may also deviate from their real values. In such a case, it would be interesting to study the stability of the coefficients $A$ and $D$ when small deviations of the parameters $\theta_{01}$, $\theta_{02}$, $\theta_{0c}$, $\theta_{0m}$, and $K$ are considered around the values used to calculate the solution given by (15). In doing so, we take one of the parameters as a variable, maintaining the rest fixed.

Each data set in Figs. 6 and 7 show the behavior of $D$ and $A$, respectively, for small changes of one of the parameters. The representation of each data set is made at those points where (16) has a physical solution, namely at those points where $w > 1$. This is the reason for having different plotting ranges from one data set to another. In the case of the coefficient $A$, we can observe its linear dependence with the relative shift $(\alpha + \delta\alpha)/\alpha$ of the parameters but, from the figure, the lack of stability of the coefficient is evident. If we now consider the behavior of the mode conversion coefficient $D$ for small shifts of the parameters $\theta_{01}$, $\theta_{02}$, $\theta_{0c}$, $\theta_{0m}$ and $K$, the dependence is also approximately linear, but in this case, the slopes of the straight lines fitting the data sets are quite small. Thus, in the case of the mode conversion coefficient $D$, we can conclude that the parameter is stable. This behavior of the coefficients $A$ and $D$ is derived from error calculus. For this purpose, let us consider the expressions of $A$ and $D$ as a function of the parameters $\theta_{0m}$ and $w$

$$D = \frac{\theta_{0m}^2}{4L} \frac{\operatorname{arccosh} w}{w\sqrt{w^2 - 1}}$$
$$A = \frac{1}{\theta_{0m}^2 L} w\sqrt{w^2 - 1} \operatorname{arccosh} w. \tag{17}$$

The parameter $w$, which has been calculated numerically, depends on $\theta_{01}$, $\theta_0$, $\theta_{0m}$, $\theta_{0c}$, and $K$. The error associated with $A$ and $D$ can be calculated according to the following expressions:

$$\Delta D = \sqrt{\left(\frac{\partial D}{\partial \theta_{0m}} \Delta\theta_{0m}\right)^2 + \left(\frac{\partial D}{\partial w} \Delta w\right)^2}$$
$$\Delta A = \sqrt{\left(\frac{\partial A}{\partial \theta_{0m}} \Delta\theta_{0m}\right)^2 + \left(\frac{\partial A}{\partial w} \Delta w\right)^2} \tag{18}$$

where $\Delta\theta_{0m}$ is the error associated with the measurement of the transition angle, and the error $\Delta w$ associated with $w$ can be calculated by means of the following formula:

$$\Delta w = \sqrt{\sum_{i=1}^{5} \left(\frac{\partial w}{\partial \alpha_i} \Delta\alpha_i\right)^2} \tag{19}$$

where $\Delta\alpha_i$ is the error associated with the parameter $\alpha_i$ ($\alpha_1 = \theta_{01}$; $\alpha_2 = \theta_{02}$; $\alpha_3 = \theta_{0m}$; $\alpha_4 = \theta_{0c}$; $\alpha_5 = K$). Note that $\Delta\theta_0 = \Delta\theta_{01} = \Delta\theta_{02}$, that is, the error committed when measuring the input angle is independent of the input angle. The

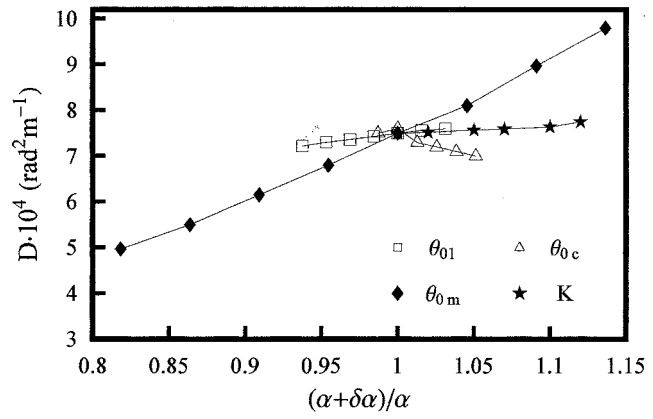


Fig. 6. $D$ as a function of the relative shift $(\alpha + \delta\alpha)/\alpha$ of the associated parameter $\alpha$ around the value used to calculate the solution given by (15). □: $\alpha = \theta_{01}$; △: $\alpha = \theta_{0c}$; ♦: $\alpha = \theta_{0m}$; ★: $\alpha = K$.

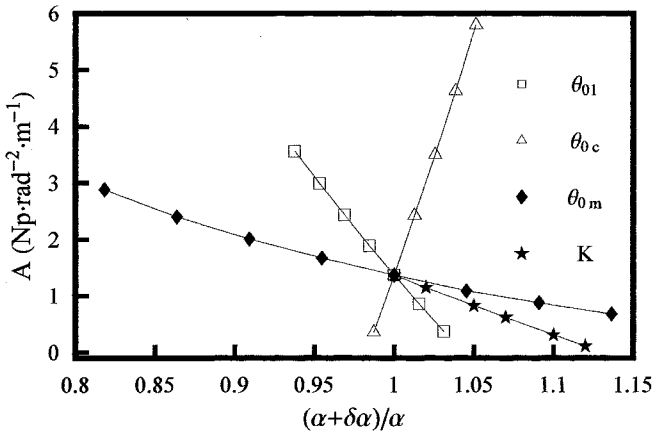


Fig. 7. $A$ as a function of the relative shift $(\alpha + \delta\alpha)/\alpha$ of the associated parameter $\alpha$ around the value used to calculate the solution given by (15). □: $\alpha = \theta_{01}$; △: $\alpha = \theta_{0c}$; ♦: $\alpha = \theta_{0m}$; ★: $\alpha = K$.

partial derivatives in (19) are estimated from the numerical solution of (16). By considering that the error committed when measuring the input angle and the transition angle is of $0.5°$ and that the error of the rest of parameters is on the order of five per cent $(\Delta\alpha_i/\alpha_i = 0.05, i = 4, 5)$, then the error estimations $\Delta D$ and $\Delta A$ are found to be

$$\Delta D = 1.4 \times 10^{-4} \text{ rad}^2/\text{m}^{-1}$$
$$\Delta A = 5 \text{ rad/m} \tag{20}$$

which give account of the relatively constant value of $D$ and the instability of the coefficient $A$.

Once we have determined $A$ and $D$ from (14), we can build the theoretical output power distribution corresponding to the input angle $\theta_0$ by using (3), and graphically compare this result with that obtained experimentally. Fig. 4 shows the theoretical curves compared with the experimental ones for the input angles of $16°$ $(\theta_{01} = 16°)$ and $21.5°$ $(\theta_{02} = 21.5°)$. The agreement is quite good, especially in the region of the peaks, as can be seen from the figure.

The main advantage of the method, in contrast to that proposed by Gambling *et al.*, is that the experimental measurements can be made over any length of fiber, while they do not need a high accuracy in the parameters involved. In fact, both long fiber lengths and the polishing conditions of the end faces have a negative influence on the results derived from the method by Gambling *et al.*: long fibers in the laboratory are wound around reels, and this may introduce additional mode coupling due to the bending of the fiber. In addition to this, the experimental conditions, and, especially, the polishing conditions are variable, since successive shorter lengths of the same fiber are required in order to determine the dependence of the transition angle $\theta_{0m}$ on length [10]. As a consequence, in the method by Gambling *et al.*, identical conditions are not obtained, and this may result in accumulative errors, especially those derived from the polishing conditions. Instead, those problems are not encountered in the method proposed in this paper, since the fiber does not need to be cut repeatedly, no matter its length, so the experimental conditions remain the same in the whole experiment.

Our method does not make use of any approximation. It only assumes, as the starting point, Gloge's coupled-power flow equation and all the assumptions involved in it. The method enables the determination of both $A$ and $D$, although the coefficient $A$ is quite sensitive to small variations in the experimental parameters, such as the input angle $\theta_0$ or the transition angle $\theta_{0m}$; thus, as happens with the method by Gambling *et al.*, our method is not appropriate for determining $A$ unless very exact experimental measurements are carried out. However, as explained before, the mode conversion coefficient $D$ is quite insensitive to these small variations.

## V. Conclusion

A simple method is proposed for the determination of the mode conversion coefficients for SI multimode optical fibers at the desired light wavelength, as an alternative to that proposed by Gambling *et al.*. It requires both measuring the far-field output pattern at the transition angle over a short fiber sample, and two additional far-field output patterns corresponding to two different launching angles, in order to determine the intersection point between them. The method assures the stability of the mode conversion coefficient $D$ to small variations of the experimental parameters around their real values. The method has been successfully tested on multimode POFs (Eska Premier fiber from Mitsubishi Co.). The results obtained from the method in this particular case and for $\lambda = 543$ nm are $D = 7.50\ 10^{-4}\text{rad}^2/\text{m}$ and an estimated error of $1.4\ 10^{-4}$ rad$^2$/m.

## References

[1] Y. Koike, T. Ishigure, and E. Nihei, "High-bandwidth graded-index polymer optical fiber," in *J. Lightwave Technol.*, L. A. Hornak, Ed. New York: Marcel Dekker, 1995, vol. 13, pp. 1475–1489. 1992, p. 1.

[2] E. Nihei, T. Ishigure, N. Tanio, and Y. Koike, "Present prospect of graded index plastic optical fiber in telecommunications," *IEICE Trans. Electron.*, vol. E-80-c, pp. 117–122, 1997.

[3] H. Murofushi, "Low loss perfluorinated POF," in *Proc. 5th Int. Conf. Plastic Optical Fibers and Applications-POF'96*, 1996, pp. 17–23.

[4] J. Zubia and J. Arrue, "Plastic optical fibers: An introduction to their technological processes and applications," *Opt. Fiber Technol.*, vol. 7, pp. 101–140, 2001.

[5] W. White, L. Blyler, G. Sherchuk, and G. Giaretta, "Routes to practical plastic optical fiber systems," in *Proc. 8th Int. POF Conf.*, 1999, pp. 92–93.

[6] R. Olshansky and D. B. Keck, "Pulse broadening in graded-index optical fibers," *Appl. Opt.*, vol. 15, pp. 483–491, Feb. 1976.
[7] R. Olshansky and S. M. Oaks, "Differential mode attenuation measurements in graded-index fibers," *Appl. Opt.*, vol. 17, pp. 1830—1835, June 1978.
[8] T. Ishigure, M. Kano, and Y. Koike, "Which is a more serious factor to the bandwidth of GI POF: Differential mode attenuation or mode coupling," *J. Lightwave Technol.*, vol. 18, pp. 959–965, July 2000.
[9] G. Jiang, R. F. Shi, and F. Garito, "Mode coupling and equilibrium mode distribution conditions in plastic optical fibers," *IEEE Photon. Technol. Lett.*, vol. 9, pp. 1128–1130, Aug. 1997.
[10] W. A. Gambling, D. P. Payne, and H. Matsumura, "Mode conversion coefficients in optical fibers," *Appl. Opt.*, vol. 14, pp. 1538–1542, July 1975.
[11] M. Rousseau and L. Jeunhomme, "Numerical solution of the coupled-power equation in step-index optical fibers," *IEEE Trans. Microwave Theory Tech.*, vol. 25, pp. 577–584, July 1997.
[12] L. Jeunhomme and J. P. Pochole, "Angular dependence of the mode-coupling coefficient in a multimode optical fiber," *Electron. Lett.*, vol. 11, pp. 425–426, Sept. 1975.
[13] L. Jeunhomme, M. Fraise, and J. P. Pocholle, "Propagation model for long step-index optical fibers," *Appl. Opt.*, vol. 15, pp. 3040–3046, Dec. 1976.
[14] J. Dugas and G. Maurel, "Mode-coupling processes in polymethylmethacrylate-core optical fibers," *Appl. Opt.*, vol. 31, pp. 5069–5079, Aug. 1992.
[15] M. Losada, I. Garces, J. Mateo, and I. Salinas, "Mode coupling in plastic optical fibers of high and low numerical apertures," in *Proc. 10th Int. Plastic Optical Fibers Conf. 2001*, 2001, pp. 109–112.
[16] D. Gloge, "Optical power flow in multimode fibers," *Bell Syst. Tech. J.*, vol. 51, pp. 1767–1783, Oct. 1972.
[17] ——, "Impulse response of clad optical multimode fibers," *Bell Syst. Tech. J.*, vol. 52, pp. 801–816, July–Aug. 1973.

**J. Zubia** received the degree in solid-state physics in 1988 and the Ph.D. degree in physics from the University of the Basque Country, Bilbao, Spain, in 1993. His Ph.D. work focused on optical properties of ferroelectric liquid crystals.

He is a Full Professor at the Telecommunications Engineering School, University of the Basque Country. He has more than eight years of experience doing basic research in the field of plastic optical fibers. At present, he is involved in research projects in collaboration with universities and companies from Spain and other countries in the field of plastic optical fibers, fiber-optic sensors, and liquid crystals.

Dr. Zubia won a Best Thesis award in 1995.

**G. Durana** received the degree in solid-state physics in 1999 from the University of the Basque Country, Bilbao, Spain, where he is currently working toward the Ph.D. degree in telecommunications engineering at the Telecommunications Engineering School.

Since 2001, he has been a Lecturer at the Telecommunications Engineering School, University of the Basque Country.

**G. Aldabaldetreku** received the M.Sc. degree in telecommunications from the University of the Basque Country, Bilbao, Spain, where he is currently working toward the Ph.D. degree in telecommunications engineering at the Telecommunications Engineering School.

His research interests are in the field of multistep optical fiber analysis, as well as polymer optical fiber modelling.

**J. Arrue** received the B.S. degree in electronic physics, the M.S. degree in electronics and telecommunications, and the Ph.D. degree in optical fibers from the University of the Basque Country, Bilbao, Spain.

He is an Associate Professor at the Telecommunications Engineering School, University of the Basque Country, Bilbao, Spain. He has been involved in international research projects for several years.

**M. A. Losada** received the Ph.D. degree in physics in 1990 from the University Complutense, Madrid, Spain.

She is an Assistant Professor at the Electronic Engineering and Communications Department, University of Zaragoza, Zaragoza, Spain. Her main research interests are in the field of fiber-optic communications.

**M. Lopez-Higuera** received the Ph.D. degree in telecommunications engineering, with an extraordinary award.

He is a Full Professor at the University of Cantabria, Spain. His main research projects are in the fields of integrated optics, optical communications, and most recently in fiber-optic sensors and smart structures.